X. Cao[a], M. Jahazi[a], H. Al-Kazzaz[b], M. Medraj[b]
[a] Aerospace Manufacturing Technology Centre, Institute for Aerospace Research, National Research Council Canada, Montreal, Canada
[b] Department of Mechanical Engineering, Concordia University, Montreal, Canada

Modelling of work-hardening behaviour for laser welded magnesium alloy

To investigate the reliability of the laser welding process for the magnesium alloy ZE41A-T5, eight butt joints were welded using the same processing parameters. These joints were tensile tested in the as-welded and aged conditions and the tensile data were analyzed from work-hardening characteristics. The flow curves cannot entirely be satisfactorily described by the Kocks–Mecking model; however, the model is still applicable to the high strain zone of the flow curves where work-hardening rate decreases linearly with flow stress. The reproducibility of the initial work-hardening rate and saturation stress is statistically analyzed. The initial work-hardening rates for the base castings and welded joints vary from approximately 4000 to 7000 MPa, i.e. 1/4 to 1/3 of the base material shear modulus. The as-welded joints have slightly higher initial work-hardening rates than the base castings. Artificial aging produces lower initial work-hardening rates compared with the base material. The saturation stress ranges approximately from 260 to 320 MPa, i.e. about 2 % of the shear modulus. The saturation stress for the welded joints is lower than that for the base material. Compared with the as-weld joints, aging decreases initial work-hardening rate but slightly increases saturation stress. Both initial work-hardening rate and saturation stress become more scattered after aging.

Keywords: Nd:YAG laser welding; Magnesium alloy; Work hardening; Kocks–Mecking model; Tensile property

1. Introduction

Accurate descriptions of stress–strain curves have been a topic of discussion for many years and many models have been developed to predict them [1–7]. The Kocks–Mecking (K–M) model has been successfully employed to describe the work-hardening behaviour for several metals and alloys including aluminium, copper, titanium, ferritic and austenitic stainless steel, and single crystals of silver [6–8]. In recent years, Tiryakioglu and his coauthors have also applied the K–M model to cast aluminium alloys [9, 10].

Some studies on the work-hardening stages of single crystals for pure magnesium and other hexagonal close packed (hcp) metals were carried out before 1980 [11]. Recently the work-hardening behaviours of commercial AZ31B-O and cast AM60 magnesium alloys, processed by LSHR (large-strain hot rolling) and ECAP (equal channel angular pressing), under different texture conditions and grains sizes, were investigated using the K–M model by means of tensile testing at room temperature [11]. It was found that the work-hardening rate (coefficient) decreases linearly with the stress in stage III, very similar to the well-known stage III behaviour in face-centred cubic (fcc) polycrystals [11]. However, little is known about the work-hardening behaviour for magnesium alloy sand castings and welded joints.

With the increasing use of magnesium alloys for structural components in aerospace, automotive, electronic and other industries, effective welding and joining methods are needed for magnesium alloys. Conventional arc welding techniques have been used, especially for repair, but laser welding is a promising technology for magnesium alloys. As a fusion technique, however, laser welding may experience similar issues such as geometrical defects, loss of chemical elements, porosity, and cracking as encountered in arc welding processes [12, 13]. Therefore, it is important to investigate the reproducibility and reliability of the laser welding process for magnesium alloys with respect to welding geometries, defects and mechanical properties. These results were reported in an earlier publication by the present authors [14]. Based on the tensile data, the attempt is made to study the work-hardening behaviour of the base magnesium alloy castings and the laser welded butt joints for two heat treatment conditions (as-welded, welded-and-aged) using the K–M model.

2. Kocks–Mecking model

Kocks has proposed an empirical work-hardening law relating the work-hardening rate to stress based on the evolution of dislocation density by thermal activation process [2, 6]. This work-hardening law was further developed by Mecking and Kocks to constitute the so-called Kocks–Mecking model. The K–M model is based on two fundamental assumptions (i) superposition of different thermal activation barriers for dislocation motion and (ii) the application of the Voce law for the evolution of work-hardening associated with dislocation accumulation and recovery [7]. The Voce equation can be expressed as [4, 5]:

$$\sigma = \sigma_s - (\sigma_s - \sigma_0) \exp\left(\frac{-\varepsilon}{\varepsilon_0}\right) \quad (1)$$

Where σ and ε are the macroscopic true stress and true plastic strains, respectively. σ_s is the saturation stress extrapolated to zero work-hardening rate (i.e. the asymptotic stress at which full plasticity is reached), σ_0 the initial or threshold

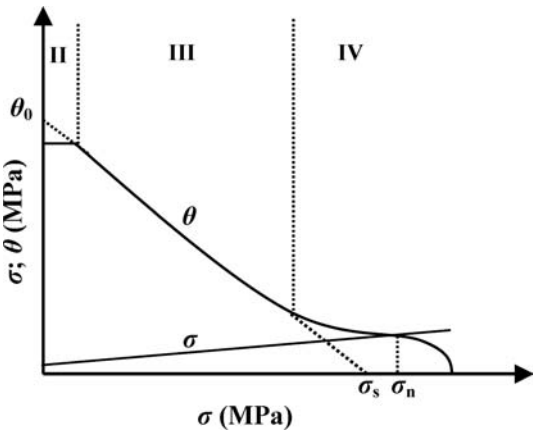

Fig. 1. Schematic relationship between work-hardening rate and true stress.

stress at which homogeneous plastic deformation begins to be appreciable [4]. σ_0 is the true stress at $\varepsilon = 0$ and usually above the limit of proportionality. Parameter ε_0 denoted by Voce [5] is a characteristic strain which determines the shape of the true stress vs. strain curve. The Voce equation constitutes the basis of the K–M model [2, 3, 6, 7]:

$$\theta = \theta_0\left(1 - \frac{\sigma}{\sigma_s}\right) \tag{2}$$

Where θ is the macroscopic work-hardening rate ($\theta = d\sigma/d\varepsilon$). The initial work-hardening rate θ_0 ($\theta_0 = \sigma_s/\varepsilon_0$) is a hardening limit extrapolated to $\sigma = 0$ [7]. The work-hardening law corresponds to stage III of plastic deformation in a polycrystalline material [7]. As schematically demonstrated in Fig. 1, stage III can often be represented by a straight line where the work-hardening rate steadily decreases linearly with stress towards a 'saturation stress σ_s'. The saturation stress is highly temperature sensitive and somewhat strain rate sensitive [15]. Stage I occurs only during single slip in single crystals. Stage II is commonly found in single crystals on low stacking fault energy materials and at low temperature at a constant, high work-hardening rate but not present in most polycrystals. The work-hardening rate in stage II is essentially constant [15]**.** When stage IV is reached, the work-hardening rate will deviate from the linear regime. The tensile instability results in necking when the Considere criterion is met, i.e. $d\sigma/d\varepsilon = \sigma$ (stress σ_n as shown in Fig. 1).

3. Experimental procedures

The experimental detail was reported in an earlier paper [14] and thus is briefly outlined here. The material was aerospace grade sand cast ZE41A-T5 (Mg-4.2Zn-1.2Ce-0.7Zr) magnesium alloy. The test specimens for laser welding had sizes of approximately $150 \times 150 \times 2.0$ mm, cut and machined from 25 mm thick sand castings. The laser welding machine used is a continuous wave (CW) 4 kW HL4006 Nd : YAG laser system. A focal length of 150 mm and a fibre diameter of 0.6 mm were employed. Helium was used to shield the top surface and argon for the bottom of the workpieces at flow rates of 18.9 and 21.2 l min^{-1}, respectively. The workpieces (butt joints) were positioned and clamped in a fixture with a gap size of 0.4 mm. A filler wire of EZ33A-T5 (Mg-3Re-2.5Zn-0.6Zr) Mg alloy with 1.6 mm diameter and 990 mm length was used through a wire feeding mechanism. The main process parameters used are laser power 4 kW, welding speed 6 m min^{-1}, wire feed rate 3.0 m min^{-1} and surface defocusing with approximately 0.45 mm focal spot diameter. The processing variables used in this work are based on the optimized process for fully penetrated butt joints of the 2 mm experimental alloy [16, 17]. To investigate the process reliability 8 butt joints were welded using the same process setup. Four randomly selected joints were artificially aged (T5) at 330 °C for 2 h immediately after laser welding. All the tensile specimens were machined according to ASTM B557M-02A, to give gauge dimensions of 10 mm width, 50 mm parallel length and 139 mm overall length. Tensile tests were carried out in an MTS-100 kN test machine fitted with a laser extensometer (25 mm gauge length was used). The tests were conducted with a cross-head speed of 0.6 mm min^{-1} (engineering strain rate 0.0004 s^{-1}) at room temperature.

The nominal values of engineering stress (S) vs. strain (e) can be converted to equivalent true stress (σ) vs. strain (ε) data using the equations: $\sigma = S(1 + e)$, and $\varepsilon = \ln(1 + e)$. The derivation of these two equations assumes both constancy of volume and a homogeneous distribution of strain along the gauge length of the tensile specimen [1]. Thus, the two equations should only be used until the onset of necking (unstable plastic flow). The true plastic strain (ε_p) can be obtained using equation $\varepsilon_p = \varepsilon - \sigma/E$ where E is Young's modulus. The work-hardening coefficient (θ) was obtained by numerical derivation of the true stress vs. true plastic strain data starting from the 0.2 % engineering yield points. In total 52 specimens were tensile tested, 24 for the as-welded, 24 for the welded-and-aged joints (T5), and 4 for the base sand castings (T5 aged).

4. Results and discussion

Figure 2 shows typical stress vs. strain curves for both the base metal (BM) and the laser-welded joints of the magnesium alloy ZE41A-T5. Both the engineering and true stresses increase with strain. None of the experimental magnesium alloy specimens, including the base sand castings and the laser welded joints in both the as-welded and the aged conditions, used in this work exhibit necking, and fracture occurs when engineering stress reaches tensile strength (TS). During the tensile plastic deformation, work-harden-

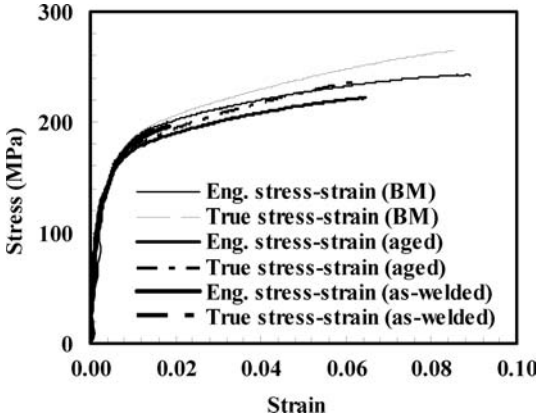

Fig. 2. Typical engineering stress vs. strain and corresponding flow curves for the base metal, and the welded joints in both the as-welded, and the aged conditions.

ing occurs since the true stress increases with strain as demonstrated in Fig. 2. In polycrystalline materials, the dislocation structure undergoes changes in the course of deformation due to the occurrence of various storage and recovery processes. Also, the increase in dislocation density as a result of plastic deformation contributes to work-hardening. On the other hand, as typically shown in Figs. 3–5, the work-hardening rate always decreases during tensile plastic deformation from the 0.2 % offset yield point indicating the lack of a pure work-hardening regime. The work-hardening rate falls quickly in the earlier period (low plastic strain zone) of the tensile plastic deformation and then decreases linearly with increasing stress. The decreasing work-hardening rate is an indication of the occurrence of dynamic recovery. Therefore, the evolution of work-hardening behaviour during tensile plastic deformation is the result of the competition between dislocation accumulation and dynamic recovery.

As indicated in Figs. 3–5, the work-hardening rate does not decrease linearly with true stress during the entire tensile plastic deformation, indicating that the K–M model cannot be used to describe the entire flow curves. In the higher stress or plastic strain zone of the flow curves, however, the macroscopic work-hardening rate decreases linearly with increasing true stress towards an apparent saturation stress, indicating that the K–M model is still valid over a significant range of the stress–strain curve. The slope of the linear portion of the θ vs. σ graphs can be related to dynamic recovery and appears to be independent of the grain size [11]. Therefore, the tensile plastic deformation in the high plastic strain regions of the flow curves can still be well described by the

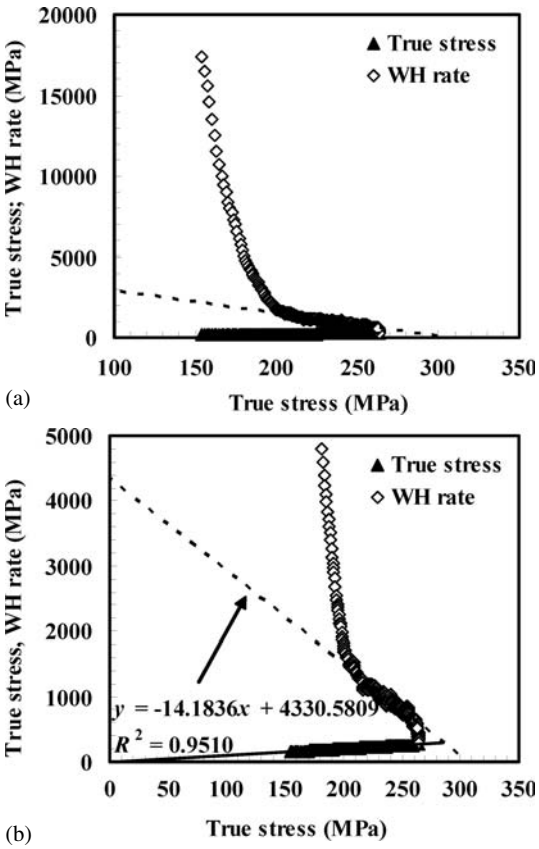

Fig. 3. (a) A typical plot for a base casting and (b) local enlargement indicating the relationship between work-hardening (WH) rate and true stress.

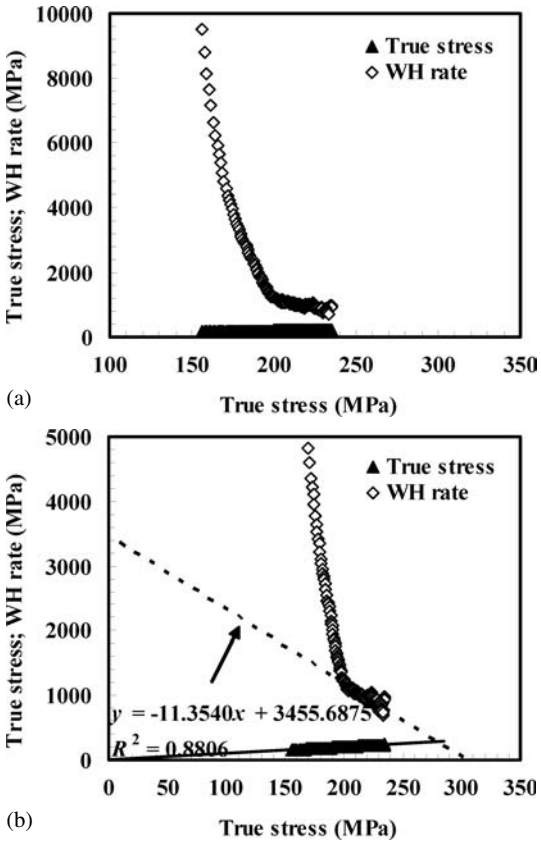

Fig. 4. (a) A typical plot for an as-welded joint fractured in the heat-affected zone and (b) local observation indicating the relationship between work-hardening rate and true stress.

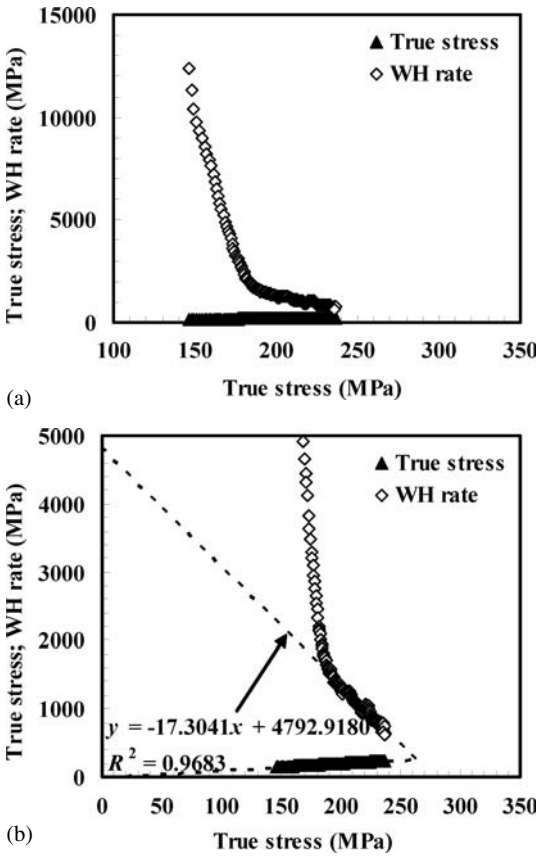

Fig. 5. (a) A typical plot for a welded-and-aged joint fractured in the fusion zone and (b) local enlargement indicating the relationship between work-hardening rate and true stress.

Voce equation as further confirmed in Fig. 6. It is also interesting to note that the Voce equation overestimates the stress at the low plastic strain zone.

Figures 7 and 8 show the frequency plots of the initial work-hardening rate θ_0 obtained from the base castings and the 2 mm laser welded butt joints in both the as-welded and the aged conditions. It was found that the initial work-hardening rates are within the same interval ranging from approximately 4000 to 7000 MPa. The statistical results are listed in Table 1. These results were obtained from 17 valid tensile curves with a well-fitted linear regime for the two heat treatment conditions, but only 3 specimens for the base material. The as-welded joints give slightly higher initial work-hardening rates than the base casting. Those with *R*-squared values less than 0.8, lack of the linear regime, or with abnormal test readings were excluded. By contrast, the aged joints have lower initial work-hardening rates than the base castings. Thus, the aging treatment decreases the initial work-hardening rates. The reproducibility of the initial work-hardening rates can be compared using the coefficient of variation. The coefficient of varia-

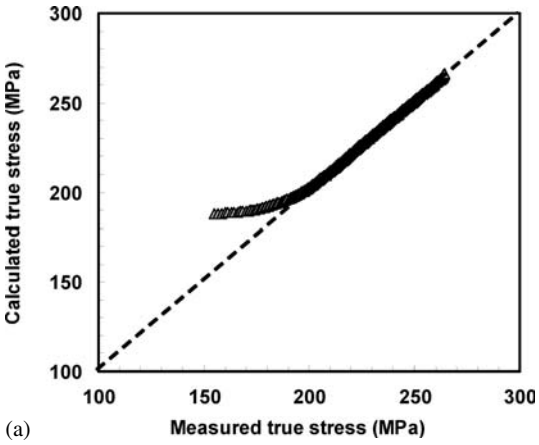

(a)

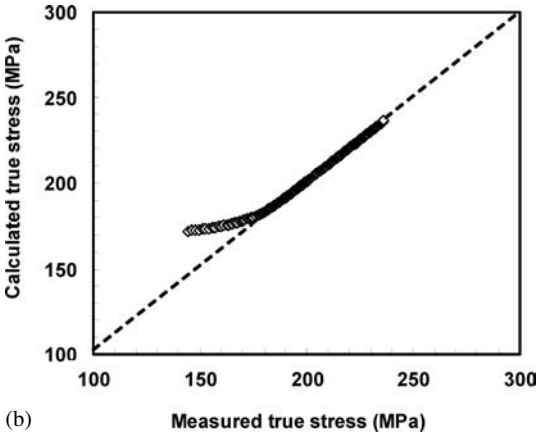

(b)

Fig. 6. Typical diagrams for (a) a base sand casting and (b) a welded-and-aged joint fractured in the fusion zone indicating the good fit of the Voce equation in the high stress or plastic strain regime.

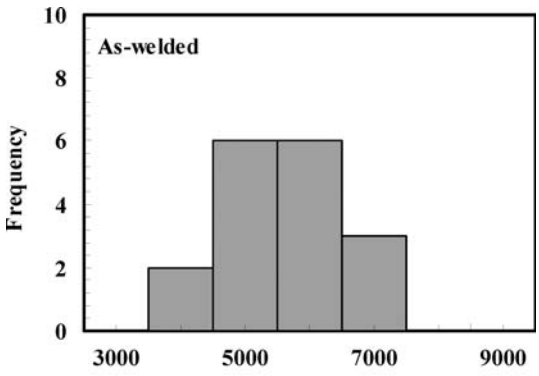

(a)

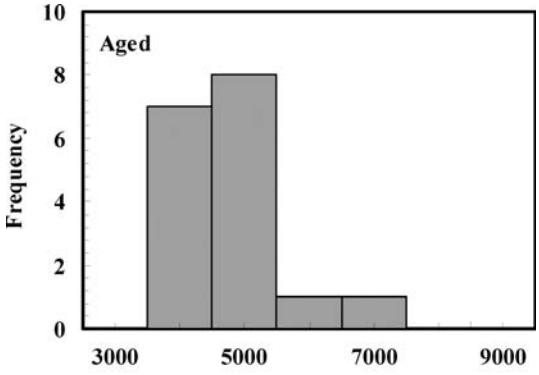

(b)

Fig. 7. Histograms of the initial work-hardening rate for the welded joints in (a) the as-welded, and (b) the welded-and-aged conditions.

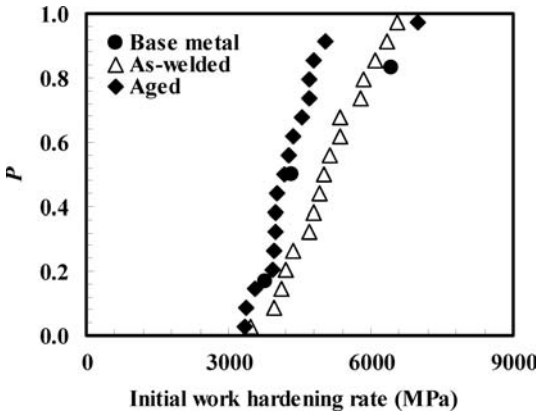

Fig. 8. Cumulative probability (*P*) distributions of the initial work-hardening rate for the base castings and the welded joints in the as-welded and the aged conditions.

Table 1. Initial work-hardening rate and saturation stress.

	Initial work-hardening rate (MPa)			Saturation stress (MPa)		
	Base castings	As-welded	Aged	Base castings	As-welded	Aged
Mean	4844.72	5054.25	4334.21	290.45	273.85	280.52
Standard deviation	1389.57	877.63	836.80	31.71	13.76	18.11
CV (%)	–	17.36	19.31	–	5.02	6.46

Note: Coefficient of variation (CV) = Standard deviation/Mean × 100 %.

tion (CV) is the percentage ratio of standard deviations to mean values [18]. CV can be used to describe how compact, or spread out a distribution of observation is and thus is a measure of scatter or dispersion of a probability distribution. This dimensionless number allows comparison of the variation of populations that have significantly different mean values, and thereby provides a method to compare the amount of variation among groups with different means. The smaller the CV, the less the scatter and the higher the reproducibility (reliability). As indicated in Table 1, the initial work-hardening rates for the aged joints are slightly more scattered than those for the as-welded joints. No comparison is made between the welded joints and base sand castings because the results for sand castings are obtained from only 3 valid tensile specimens.

Kocks [6] investigated polycrystalline high-purity aluminium at various temperatures and two strain rates. It was found that the θ_0/μ value (μ is temperature-dependent shear modulus) converges towards a finite value which is insensitive to temperature and strain rate [6]. The same is true for polycrystalline high-purity copper and commercial type 304 stainless steel over temperature ranges up to about $0.6\,T_M$ (T_M is the absolute melting temperature) though there is some scatter around this constant value for stainless steel [6]. Therefore, the initial work-hardening rate is insensitive to temperature and strain rate for cubic lattice metals. This initial work-hardening rate is approximately between 1/20 and 1/15 of the material shear modulus [6]. For the ZE41A-T5 magnesium alloy used in this work, Young's modulus $E = 44\,000$ MPa, and Poisson's ratio $\upsilon = 0.35$. Thus the shear modulus $G = E/2(1 + \upsilon) \approx 16\,300$ MPa. The initial work-hardening rate for the ZE41 sand castings and the laser welded joints ranges approximately from 1/4 to 1/3 of the material shear modulus. Therefore, the ratio of the initial work-hardening rate to the material shear modulus for hcp structure magnesium alloys is 5 times that of cubic lattice structure metals.

Another characteristic parameter, saturation stress σ_s, at which the work-hardening rate tends to be zero, is presented in Figs. 9 and 10. Almost all the saturation stresses lie in a similar window ranging from approximately 260 to 320 MPa for the base castings and the welded joints in both the as-welded and the aged conditions. The saturation stress for the welded joints is slightly lower than that for the base castings. The aging treatment can slightly increase the saturation stress but the distribution of the saturation stress becomes more scattered compared with the as-welded condition.

It has been reported that the saturation stress can be reduced by increasing the temperature and, at a given temperature, by decreasing the strain rate with the effect of temperature being more pronounced [6]. The mechanical saturation stress (which would be approached at absolute zero temperature) is independent of strain rate and varies between about 0.6 % and 3 % of the material shear modulus for various polycrystalline materials such as aluminium, copper and stainless steel. The higher values for these materials are due to lower stacking-fault energy [6]. In the present work, the saturation stress at room temperature for the ZE41 sand castings and the welded joints is approximately 2 % of the material shear modulus, being consistent with the mechanical saturation stress at absolute zero temperature for cubic lattice metals.

Figure 11 shows the relationship between the initial work-hardening rate and saturation stress. Generally speaking, higher saturation stress is obtained at lower initial work-hardening rates, i.e. saturation stress tends to decrease with increasing initial work-hardening rate. Although all experiments in this work were carefully controlled and conducted, the variation in the initial work-hardening rate and saturation stress may be an indication of welding process reliability for the hcp structure magnesium alloy.

Compared with the as-welded joints, the aging treatment decreases the initial work-hardening rate and increases the saturation stress. After aging, the two parameters become more scattered. This is in agreement with the reproducibil-

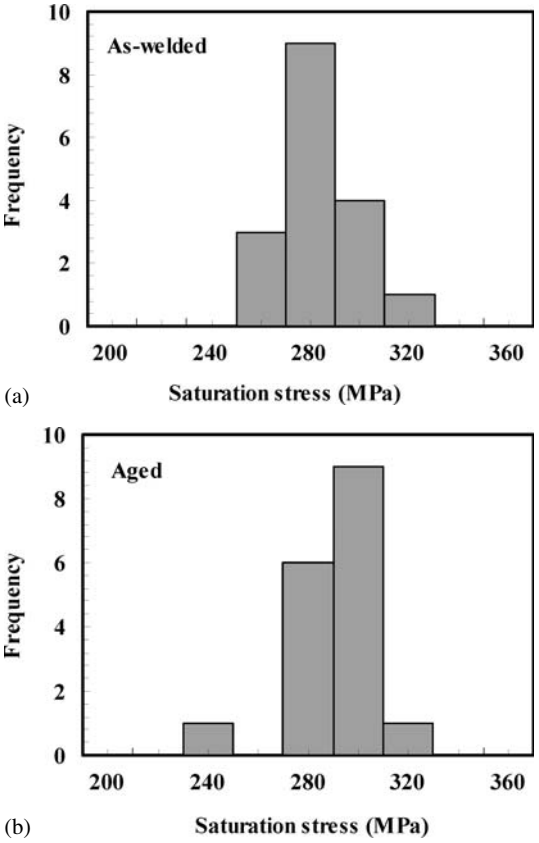

Fig. 9. Histograms of the saturation stress for the welded joints in (a) the as-welded and (b) the welded-and-aged conditions.

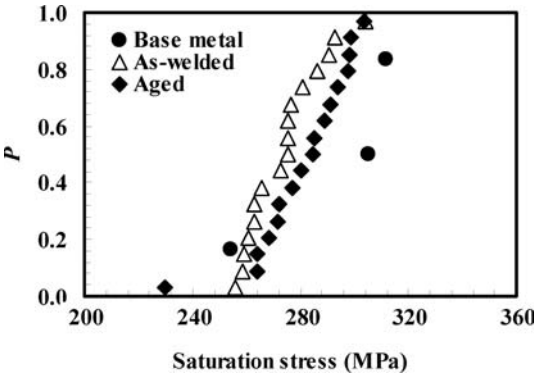

Fig. 10. Cumulative probability distributions of the saturation stress for the base castings and the welded joints in the as-welded and the aged conditions.

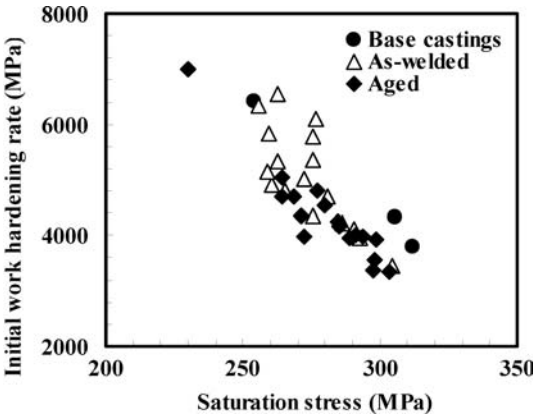

Fig. 11. Relationship between the initial work-hardening rate and saturation stress.

ity of conventional tensile properties [14]. After the aging treatment, the mechanical properties become more scattered since lower Weibull modulus values for tensile strength and fracture elongation were obtained (The Weibull modulus is roughly the inverse of the coefficient of variation for a Weibull-type distribution). This further indicates that the aging treatment is probably not necessary for ZE41A-T5 sand castings after laser welding, though it may relieve some residual stresses.

As discussed above, the Kocks–Mecking model is not applicable to the entire work-hardening curves of magnesium alloys but still quite valid for the high stress or plastic deformation zone of the flow curves. These regimes are important because they are the zones immediately prior to the failure of the tensile specimens. Thus the K–M model may provide an approach to investigate the failure behaviour of magnesium alloy welded joints. It is expected that the mechanical properties of the weld joints in the absence of macrodefects might be predicted from the work hardening behaviour.

5. Conclusions

The applicability of work-hardening behaviour of 2 mm magnesium alloy ZE41A-T5 sand castings and laser welded butt joints in the as-welded and aged conditions, was investigated using the Kocks–Mecking model through room temperature tensile tests.

1. The high stress or plastic strain zones of the flow curves can be satisfactorily described by the Kocks–Mecking model. In this regime the work-hardening rates decrease linearly with the flow stress.
2. The initial work-hardening rate for the ZE41 sand castings and the welded joints varies from approximately 4000 to 7000 MPa, i.e. 1/4 to 1/3 of the material shear modulus. The as-welded joints have slightly higher initial work-hardening rate than the base sand castings. Aging treatment produces lower initial work-hardening rate compared with the base castings.
3. The saturation stress for the base ZE41 sand castings and welded joints varies from approximately 260 to 320 MPa, i.e. about 2 % of the shear modulus. The saturation stress for the welded joints is lower than that for the base castings.
4. Compared with the as-welded joints, the aging treatment decreases the initial work-hardening rate by approximately 14 % but slightly increases the saturation stress by approximately 2.5 %. After the aging treatment, both the initial work-hardening rate and the saturation stress become more scattered. This is in agreement with more scattered tensile strength and fracture elongation values observed after the aging treatment.

The authors would like to thank Dr. M. Xiao for the preparation of the welded joints using 4 kW Nd:YAG laser welding system. Thanks are also due to Dr. M. Tiryakioglu for the useful discussion.

References

[1] G.E. Dieter: Mechanical Metallurgy, 3rd Ed., McGraw-Hill Book Company, New York (1986).
[2] U.F. Kocks, H. Mecking: Prog. Mater. Sci. 48 (2003) 171.
[3] E. Nes: Prog. Mater. Sci. 41 (1998) 129.
[4] E. Voce: J. Inst. Met. 74 (1948) 537.
[5] E. Voce: Metallurgia 51 (1955) 219.
[6] U.F. Kocks: J. Eng. Mater. Tech. 98 (1976) 76.
[7] N. Tsuchida, Y. Tomota, H. Moriya, O. Umezawa, K. Nagal: Acta Mater. 49 (2001) 3029.
[8] C.G. Shastry, M.D. Mathew, K.B.S. Rao, S.L. Mannan: Int. J. Pressure Vessels Piping 81 (2004) 297.
[9] M. Tiryakioglu: Mater. Sci. Eng. A 427 (2006) 154.
[10] M. Tiryakioglu, J. Campbell, J.T. Staley: Mater. Sci. Eng. A 368 (2004) 205.
[11] J.A. del Valle, F. Carreno, O.A. Ruano, Acta Mater. 54 (2006) 4247.
[12] X. Cao, M. Xiao, M. Jahazi, J.P. Immarigeon: Mater. Manufact. Processes 20 (2005) 987.
[13] X. Cao, M. Jahazi, J.P. Immarigeon, W. Wallace: J. Mater. Process. Technol. 171 (2006) 188.
[14] H. Al-Kazzaz, X. Cao, M. Jahazi, M. Medraj: Metall. Trans., submitted (2007).
[15] A.D. Rollett, U.F. Kocks, in: Proc. "Dislocation-93" Conf., Aussois, France, April 1–9, 1993.
[16] H. Al-Kazzaz, M. Medraj, X. Cao, M. Jahazi, M. Xiao, in: J.P. Marttin (Ed.), Proc. Int. Symp. on Light Metals, pp. 137–149, COM 2005: 44th Annual Conf. Of Metallurgists of CIM, Calgary, Albert, Canada, Aug. 21–24, 2005.
[17] H. Al-Kazzaz, M. Medraj, X. Cao, M. Jahazi, M. Xiao, in: M.O. Pekgulerguz, L.W.F. Mackenie (Eds.), Magnesium Technology In the Global Age, pp. 503–518, COM 2006: 45th Annual Conf. Of Metallurgists of CIM, Montreal, Canada, 1–4 Oct. 2006.
[18] X. He, S.O. Oyadiji: J. Mater. Process. Tech. 119 (2001) 374.

(Received May 17, 2007; accepted 22, 2007)

Bibliography

DOI 10.3139/146.101622
Int. J. Mat. Res. (formerly Z. Metallkd.)
99 (2008) 2; page 216–221

ISSN 1862-5282

Correspondence address

Dr. Xinjin Cao
Research Officer
Aerospace Manufacturing Technology Center
Institute for Aerospace Research, National Research Council Canada
5145 Decelles Avenue, Montreal, Quebec, Canada, H3T 2B2
Tel.: +1 514 283 9047
Fax: +1 514 283 9445
E-mail: Xinjin.cao@cnrc-nrc.gc.ca